J. Jpn. Soc. Powder Powder Metallurgy, **72** (2025) S997-S1001
https://doi.org/10.2497/jjspm.15P-T21-07

Strain Analysis of Thermoelectric Materials using High-resolution Synchrotron X-ray Diffraction Data

Hayato NAKASAWA[1]*, Takahisa SHOBU[2], Aki TOMINAGA[2], Masashi FUJII[1], Hironari MATSUMOTO[1], Michiko MATSUDA[1], Takeshi SHIMADA[1], Vikrant TRIVEDI[3], Makoto TACHIBANA[3], Naohito TSUJII[3] and Takao Mori[3]

[1]Proterial, Ltd. Global Research and Innovative Technology Center, 5200 Mikajiri, Kumagaya-shi, Saitama 360-8577, Japan.

[2]Materials Science Research Center, Japan Atomic Energy Agency, 1-1-1 Kouto, Sayo-cho, Sayo-gun, Hyogo 679-5148, Japan.

[3]Research Center for Materials Nanoarchitectonics, National Institute for Materials Science, 1-1 Namiki, Tsukuba, Ibaraki 305-0044, Japan.

Abstract

A compressive strength limit is one of critical parameters for thermoelectric materials. In this study, we synthesized a single crystal of Yb-filled Co–Sb-based skutterudite. We assessed the compressive pressure dependence of internal strain using high-resolution synchrotron radiation X-rays at SPring-8. The prepared single crystal was identified as $Yb_{0.148}Co_4Sb_{12.54}$, with a lattice parameter of 9.0504 Å. Compressive testing was performed until the sample fractured, revealing a compressive strength limit of 591.3 MPa. The stress–strain curve exhibited a nearly constant slope for strains exceeding 0.07%, leading to an estimated Young's modulus of 154.6 GPa.

Keywords: Co–Sb based skutterudite, Sb-flux method, compressive strength limit, in situ strain measurement method

Introduction

Thermoelectric generation has attracted attention as a crucial technology for transitioning to a carbon-neutral society because it can directly convert exhaust heat into electric power[1)]. It is essential to assemble modules using materials with a high figure-of-merit zT to construct an efficient thermoelectric generator because this directly influences conversion efficiency. Skutterudite-based materials (SKD) are particularly promising in this regard, exhibiting a zT exceeding 1[2,3)], mechanical robustness[4)], and affordability[5)]. For future industrial applications, most research of SKD primarily have focused on improving zT, and recent studies have achieved zT enhancements exceeding 1.7 through techniques such as multi-filling[6,7)], nanopores[8)], and nano-composites[9)]. However, a comprehensive understanding of the fundamental mechanical properties of skutterudites, particularly the stress–strain curve, remains limited owing to challenges associated with accurate measurement. In industrial applications aiming for high-efficiency generation, thermoelectric devices are often pressed tightly against hot or cold sources to create substantial thermal gradients across the modules. This can subject the component materials to compressive stress as a result. Therefore, understanding the compressive strength limit derived from the stress–strain curve of materials is valuable in the field of thermoelectrics.

Previous computational studies for skutterudites using molecular dynamics have predicted the compressive strength limit[10-12)]. However, these calculations typically focus on the unfilled-SKD simple structure owing to the considerable computational costs of evaluating filled-SKD complex structures. Additionally, synthesizing filled-SKD materials is complex because they exist as metastable phases, often requiring quenching, melt-spinning, sintering using methods such as spark plasma sintering to achieve homogeneous compounds[13,14)]. Owing to these challenges, there have been limited theoretical and experimental investigations into the mechanical properties of filled-SKD materials. In this study, a uniaxial compressive test was performed on single crystal filled-SKD specimens to understand these mechanical properties. The internal strain during compression was evaluated using X-ray diffraction (XRD) with an in situ strain measurement method[15)]. Specifically, hard X-rays generated at the large synchrotron radiation facility SPring-8 were utilized for this XRD evaluation. Unlike conventional XRD methods that use X-ray Cu tubes and typically detect reflection data from surface layers up to a few micro-millimeters deep, synchrotron high-energy X-rays offer deep penetration depths. This results in obtaining reflections from through-thickness diffraction planes within the crystal. Recently, advancement in synchrotron XRD imaging have enabled real-time and real-space studies of fracture mechanics near the speed of sound, providing direct observations of crack propagation[16)]. Therefore, synchrotron XRD is a powerful technique specialized for measuring internal bulk strain, complementing traditional XRD methods.

Experiment

Evaluating internal strain

In Fig. 1, we illustrate the non-destructive evaluation of internal strain performed using the in situ strain measurement method[15)], employing synchrotron radiation X-rays at SPring-8. Specifically, we utilized monochromatic X-ray from the BL22XU beamline, with a photon energy of 69.42 keV, a CsI scintillator, and a charge-coupled device (CCD) camera as a 2D detector. The incident slits were set to size of 0.2 × 0.2 mm^2. XRD measurements were performed by tilting (ψ) the specimen to scan multiple diffraction spots. The estimation of specimen strain was performed according to the following equation

$$\varepsilon = \Delta d/d_0 = (\theta_0 - \theta) / \tan \theta_0 \quad \ldots. (1)$$

where ε is the strain, d is the lattice spacing, and θ and θ_0 are the diffraction angles under load and in the stress-free state, respectively. The strain is determined by accurately measuring θ, with a scanning increment of θ set to 0.002°. A sample holder illustrated in Fig. 2 was utilized for the destructive compressive test. Fig. 3 demonstrates the progressive increase in applied load until the sample fractures, with XRD measurements performed at interval of 50 N.

*Corresponding author E-mail: hayato.nakasawa.ge@proterial.com

Crystal synthesis and processing

A single crystalline sample of $Yb_xCo_4Sb_{12}$ was grown via the Sb-flux method, employing high-purity Yb-grains (99.9%, Rare Metallic Co., Japan), and Co-grains (99.97%, Rare Metallic Co., Japan), and Sb-shots (99.9999%, Kojundo Chemical Co., Japan) as starting materials. These materials were combined in an Al_2O_3 crucible with an excess amount of Yb and Sb (Yb:Co:Sb = 2:4:46), then sealed in an evacuated quartz tube under a 10^{-3} Pa vacuum. The ampule was heated at 1273 K for 12 h to melt the starting materials, followed by a controlled cooling down to 943 K at a rate of 3.3 K/h to facilitate crystal growth. Subsequently, the ampule was maintained at 943 K for a few hours for annealing to reduce residual stress and defects, after which the excess flux was removed by centrifugation. The obtained crystal was characterized using electron probe X-ray microanalysis (EPMA; JXA-8500F, JEOL, Japan). A single crystalline sample of $YbSb_2$ was previously prepared and used as the standard for the chemical composition analysis of Yb and Sb. In contract, a metal Co sample served as the standard for Co. EPMA was performed with an acceleration voltage of 15 kV and a probe current of 100 nA. For the synchrotron XRD measurement, the crystal specimen was sliced into a cuboid measuring 1 × 1 × 1 mm along the [100] axis and then affixed to a zirconia column base.

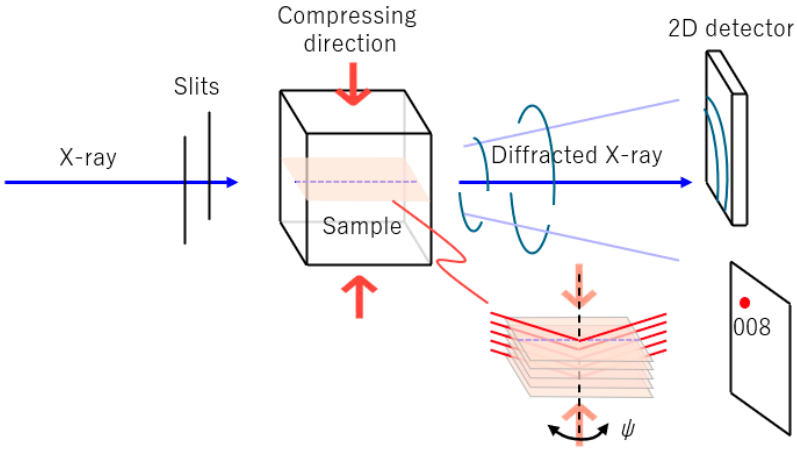

Fig. 1 Schematic illustration of strain measurement using synchrotron radiation X-rays

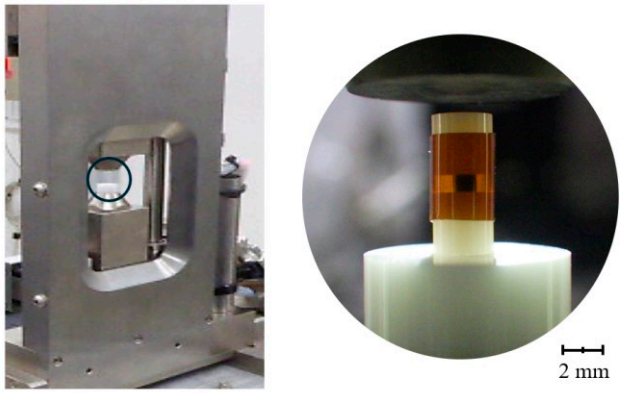

Fig. 2 Sample holder and sample for compressive test

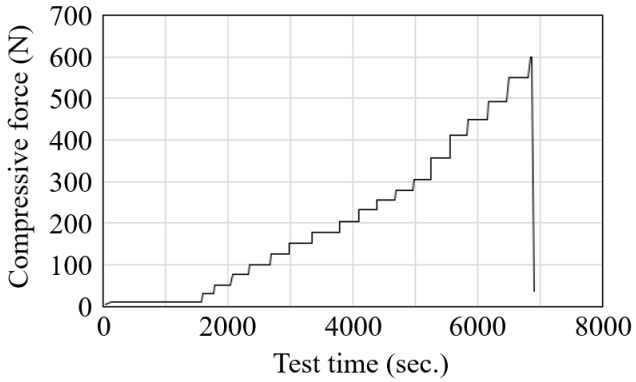

Fig. 3 Time dependence of load in the compressive test

Results and Discussion

Fig. 4 presents photographs of the crystalline sample obtained via the Sb-flux method, showcasing the skutterudite phase and residual Sb before processing. Through EPMA characterization, the SKD phase was identified as $Yb_{0.148}Co_4Sb_{12.54}$, revealing a lower Yb content compared to the targeted composition of $Yb_{0.3}Co_4Sb_{12}$. The XRD pattern of the single crystalline sample is depicted in Fig. 5 alongside the polycrystalline XRD pattern of $Yb_{0.3}Co_4Sb_{12}$. By stacking diffraction images via tilting the normal vector of {001}, a Laue pattern comprising individual Laue spots was clearly obtained, indicating uniform crystalline quality within the beam size of 2 × 0.2 × 0.2 mm during measurement. The one-dimensional diffraction profile along the [100] direction, illustrated in Fig. 6, reveals four high-intensity peaks corresponding to [100] plane reflections. From the data of the identified (008) peak, the interplanar distance d and lattice parameter a were determined and summarized in Table 1 along references. The lattice parameter of $Yb_{0.148}Co_4Sb_{12.54}$ was 0.2% larger than that of single crystal $CoSb_3$ in previous studies[17,18]. This observation suggests an expansion in the unit cell volume of SKD owing to filling[19-21], with the Yb component occupying vacancy sites in the $CoSb_3$ structure.

Table 1. Estimated inter-planar distance d and lattice parameter a of single crystal

actual composition	ref. peak	2θ (deg.)	d (Å)	a (Å)
$Yb_{0.148}Co_4Sb_{12.54}$	(008)	9.0547(1)	1.1313	9.0504(1)
p-Co_4Sb_{12} [17]				9.0345(3)
p-Co_4Sb_{12} [18]				9.03626(5)

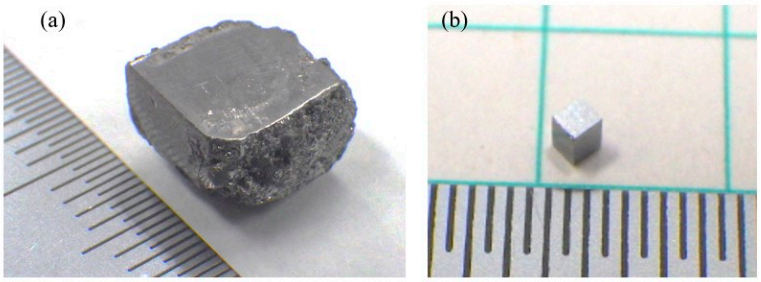

Fig. 4 $Yb_{0.3}Co_4Sb_{12}$ crystal sample (a) before processing (7 × 7 × 6 mm) and (b) after processing (1 × 1 × 1 mm)

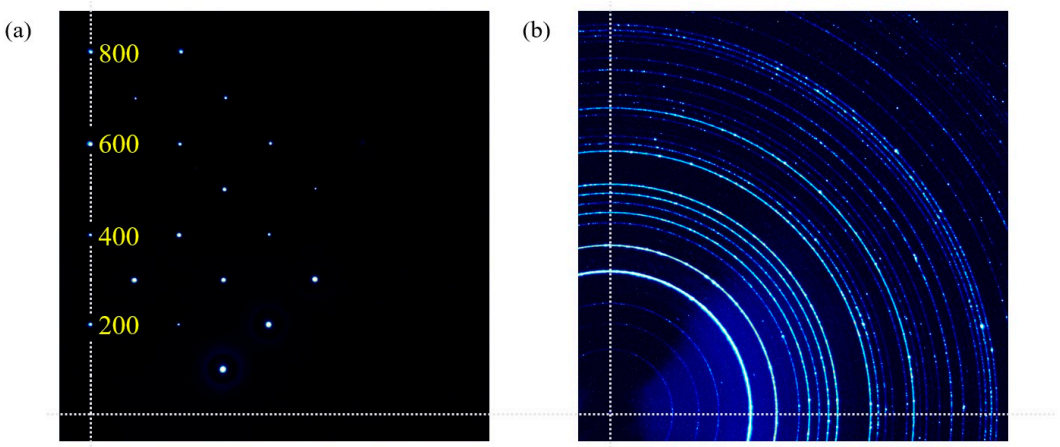

Fig. 5 (a) XRD pattern of single crystal $Yb_{0.148}Co_4Sb_{12.54}$ and (b) XRD pattern of polycrystalline $Yb_{0.3}Co_4Sb_{12}$

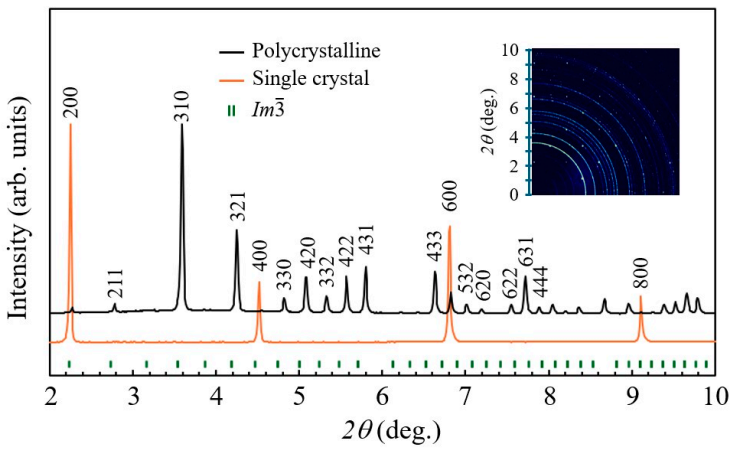

Fig. 6 Diffraction profiles of single crystal sample and polycrystalline sample of $Yb_{0.3}Co_4Sb_{12}$.

Fig. 7 shows the (800) diffraction profiles of the single crystalline sample under compression loading. To accurately observe peak positions, the high diffraction-angle (008) reflection was selected as a reference peak. With increasing load, the peak angle was shifted higher, eventually reaching to 9.0739(1)° from 9.0547(1)° when the load reached 550 N. Such shifts in the peak position during compression typically indicate lattice contraction, signifying larger compressive strain. In this study, the internal strain was evaluated using equation (1) with d_{10N} = 1.1313 Å as the reference d_0. The strain values are plotted in Fig. 8 alongside compressive stress, which was calculated based on the actual bottom area size of 0.9301 mm^2. It was observed that until the compressive strain exceeded 0.07%, the approximation did not properly align with the stress–strain curve. This discrepancy was attributed to inaccuracies in sample processing, highlighting the need for revisiting surface flattening techniques to achieve linearity in the stress–stain curve at low strains below 0.07%. Conversely, in the compressive strain range from 0.07% to 0.2%, the curve exhibited a nearly constant slope before reaching the yield limit. This linear relationship in the stress–strain curve indicates that the single crystal of SKD can deform elastically in this strain range. The slope value in the stress–strain linear relationship, known as Young's modulus E, was determined to be 154.6 GPa, closely corresponding to reported experimental values of polycrystalline CoSb3[11,22,23]. Upon reaching a load of 550 N, the internal strain exceeded 0.2%, and the compressive stress reached 591.3 MPa without fracturing. Subsequently, although the sample withstood a compression of 645.1 MPa for 20 s (Fig. 3), it fractured before XRD measurement could commence after the load reached 600 N.

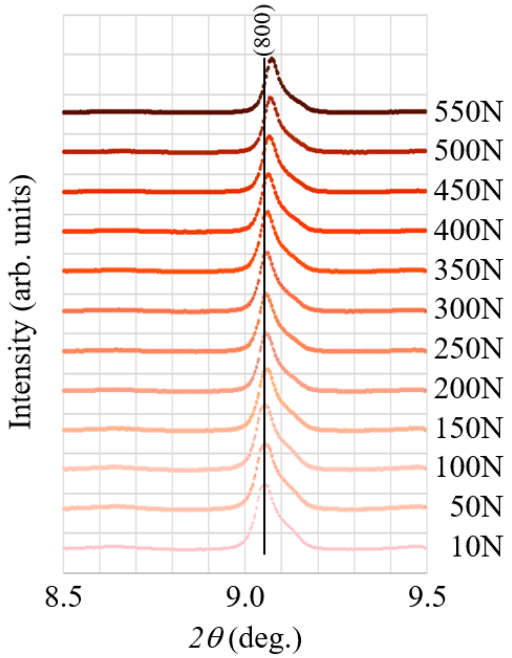

Fig. 7 XRD profiles of single crystal with increasing load

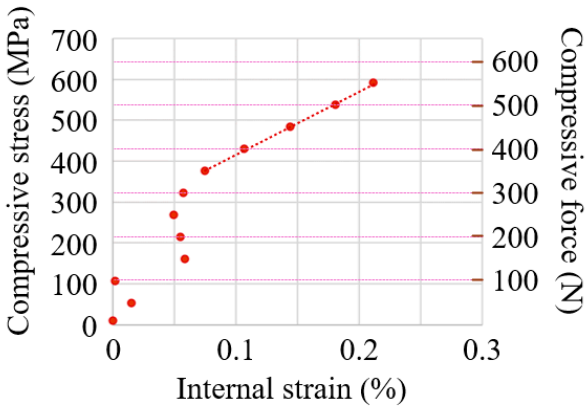

Fig. 8 Stress–strain curve of single crystal

Conclusion

In this study, we synthesized a single crystal of Yb-filled Co–Sb-based skutterudite. We investigated the compressive pressure dependence of internal strain using high-resolution synchrotron radiation X-rays at SPring-8. The single crystalline sample exhibited uniform crystalline quality and was characterized as $Yb_{0.148}Co_4Sb_{12.54}$ through EPMA measurements. Employing the in situ strain measurement method with synchrotron radiation XRD, we identified a linear relationship in the stress–strain curve with a constant slope of 154.6 GPa. for strain value exceeding 0.07%. The crystal failed completely when the compression load reached 600 N, leading to an estimated compressive strength limit of 591.3 MPa for $Yb_{0.148}Co_4Sb_{12.54}$. This non-destructive evaluation for strain using synchrotron radiation XRD technique is promising for application in thermoelectric materials and in various functional materials crucial for future society.

Acknowledgements

The synchrotron radiation experiments were performed at the BL22XU of SPring-8 with the approval of the Japan Atomic Energy Agency under the proposal No. 2022B3726, 2023A3721, and 2023B3722. This project was supported by JST Mirai Program Grant JPMJMI19A1.

References

1) T. Hendricks, T. Caillat and T. Mori: Energies, **15** (2022) 7307 1-35.
2) C. Uher: Thermoelectric Skutterudites, CRC Press: Boca Raton, USA, (2021).
3) R. Freer et al.: J. Phys.: Energy, **4** (2022) 022002 1-130.
4) G. Rogl and P. Rogl: Sci. Adv. Mater., **3** (2011) 517-538.
5) X. L. Shi, J. Zou and Z. G. Chen: Chem. Rev., **120** (2020) 7399-7515.

6) G. Rogl, A. Grytsiv, K. Yubuta, S. Puchegger, E. Bauer, C. Raju, R. C. Mallik and P. Rogl: Acta Mater., **95** (2015) 201-211.
7) G. Rogl, A. Grytsiv, F. Failamani, M. Hochenhofer, E. Bauer and P. Rogl: J. Alloys Compd., **695** (2017) 682-696.
8) A. U. Khan, K. Kobayashi, D. Tang, Y. Yamauchi, K. Hasegawa, M. Mitome, Y. Xue, B. Jiang, K. Tsuchiya, D. Golber, Y. Bando and T. Mori: Nano Energy, **31** (2017) 152-159.
9) W. Zhao, Z. Liu, Z. Sun, Q. Zhang, P. Wei, X. Mu, H. Zhou, C. Li, S. Ma, D. He, P. Ji, W. Zhu, X. Nie, X. Su, X. Tang, B. Shen, X. Dong, J. Yang, Y. Liu and J. Shi: Nature, **549** (2017) 247-251.
10) X. Q. Yang, P. C. Zhai, L. S. Liu, and Q. J. Zhang: J. Appl. Phys., **109** (2011) 123517 1-6.
11) J. Li, X. Zhang, B. Duan, G. Li, Y. Ma and H. Xu: Mater. Today Commun., **38** (2024) 107761 1-5.
12) W. Li, G. Li, X. Yang, L. Liu and P. Zhai: J. Electron. Mater., **44** (2015) 1477-1482.
13) H. Li, X. Tang, Q. Zhang and C. Uher: Appl. Phys. Lett., **93** (2008) 252109 1-3.
14) Y. Shiota, Y. Ohishi, M. Matsuda, T. Shimada, A. Nambu and H. Muta: J. Alloys Compd., **829** (2020) 154478 1-6.
15) T. Shobu, H. Konishi, J. Mizuki, K. Suzuki, H. Suzuki, Y. Akiniwa and K. Tanaka: Mater. Sci. Forum, **524-525** (2006) 691-696.
16) M. G. Tsoutsouva, G. Regula, B. Ryningen, P. E. Vullum, N. Mangelinck-Noël, G. Stokkan: Acta Mater., **210** (2021) 116819 1-11.
17) T. Caillat, A. Borshchevsky and J. P. Fleurial: J. Appl. Phys., **80**(8) (1996) 4442-4449.
18) M. Pillaca, O. Harder, W. Miller and P. Gille: J. Cryst. Growth, **475** (2017) 346-353.
19) S. Wang, J. R. Salvador, J. Yang, P. Wei, B. Duan and J. Yang: NPG Asia Mater., **8** (2016) e285 1-11.
20) J. Nagao et al.: J. Appl. Phys., **92**(7) (2002) 4135-4137.
21) P. F. Qiu, J. Yang, R. H. Liu, X. Shi, X. Y. Huang, G. J. Snyder, W. Zhang and L. D. Chen: J. Appl. Phys., **109** (2011) 063713 1-8.
22) V. Ravi, S. Firdosy, T. Caillat, B. Lerch, A. Calamino, R. Pawlik, M. Nathal, A. Sechrist, J. Buchhalter and S. Nutt: AIP Conf. Proc., **969** (2008) 656-662.
23) P. Wen, H. Mei, P. Zhai and B. Duan: J. Mater. Eng. Perform., **22** (2013) 3561-3565.

Received June 28, 2024; Revised September 3, 2024; Accepted September 3, 2024